ELSEVIER

Ceramics International 33 (2007) 89–93

CERAMICS INTERNATIONAL

www.elsevier.com/locate/ceramint

Modified glycine nitrate procedure (MGNP) for the synthesis of SOFC nanopowders

Snezana B. Bošković [a,*], Branko Z. Matovic [a], Milan D. Vlajić [b], Vladimir D. Kristić [b]

[a] *Institute of Nuclear Sciences Vinča, 11001 Belgrade, POB 522, Materials Sciemce Laboratory, Serbia and Montenegro*
[b] *Centre for Manufacturing of Advanced Ceramics and Nanomaterials, Queens University, CMACN Queen's University, Nicol Hall, Kingston, Ont., Canada*

Received 21 April 2005; received in revised form 18 June 2005; accepted 29 July 2005
Available online 29 September 2005

Abstract

Nanopowders with perovskite type crystal structure were synthesized by modified glycine nitrate procedure. Modification of the procedure was performed by partial replacement of nitrates by acetates, in order to control the burn-up reaction. The obtained nanopowders, according to XRD results are single phase, independent of number of dopants. The yield of powder in all cases was very close to the theoretical one. Many different powders with perovskite type crystal structure were produced, with cation dopants on A as well as on B sites or both. Properties of the synthesized powders together with sintering tests are discussed.

Keywords: MGNP-modified glycine nitrate procedure; Nanosized powders; SOFC

1. Introduction

There are numerous reasons for which SOFC are in a focus of interest, the most important ones being high efficiency, low emission of pollutants, and consequently the development of sustainable energy sources [1–4]. Important trend in SOFC development is to decrease the cost of powder production, whereby homogeneous, clean, nanosized powders with precise stoichiometry should be synthesized. Also, very important feature is to develop the method that will be reliable as far as powder properties are concerned.

The major objective of this paper is to present results on highly effective and simple procedure for synthesis of powders, which are good candidates for SOFC components. Both doped Ca-manganates, as well as, Ba-cerates, as a new generation of materials for future SOFC were synthesized. The procedure we used is both time- and cost effective.

The glycine nitrate process [5,6], a self-combustion method for powder synthesis, uses amino acetic acid (glycine) as a fuel and metal nitrate of the composition to be synthesized, as an oxidant. In our work, however, this method had been modified to give the possibility of producing very fine, very clean, nanometric powders in a very short time, with the yield of 98–99%. According to our knowledge, there are no similar data in the literature. Many different powders with perovskite type crystal structure—manganates and cerates—were produced, containing cation dopants on A as well as on B sites or both. Sintering tests were performed, as well, and these results are included, too.

2. Experimental

2.1. Synthesis

Starting chemicals used for the synthesis of powders were aminoacteic acid–glycine (Fischer Scientific, USA), metallic acetates (Mn, Ba) and nitrates (Ce, La, Y, Nd, Gd, Sm), produced by Aldrich, USA. Synthesis was carried out in a stainless steel reactor in which all reactants dissolved in distilled water were added according to previously calculated composition of the final powder. We used nitrates in the form of solutions, and acetates in the as received form. Glycine was also added in the as received form. As an example, the amount of chemicals dissolved in distilled water for $BaCe_{0.9}Gd_{0.1}O_3$ powder preparation is given:

* Corresponding author. Tel.: +381 11 2439454; fax: +381 11 2439454.
E-mail address: boskovic@vin.bg.ac.yu (S.B. Bošković).

0272-8842/$30.00
doi:10.1016/j.ceramint.2005.07.022

Ba-Acetate: 51.09 g
$Ce(NO_3)_3{\cdot}6H_2O$: 172.44 ml (1.009 molarity)
$Gd(NO_3)_3{\cdot}6H_2O$: 22.6 ml (0.8906 molarity)
Glycine: 30 g, water: 250 ml
Water: 250 ml

The reactants were heated on a hot plate up to about 540 °C, until the evolution of the smoke terminated. As a result of modifying GNP, the reaction proceeded very smoothly. Therefore, almost no loss in the synthesized powders quantity was observed. The experimentally obtained amount of powder was very close to the theoretically calculated one, 96–99%. For practical reasons, it is very important to outline that the quantity of chemicals was designed to synthesize 100 g of powder per run (in 30 min), which is according to our knowledge among the largest scale produced by this method so far. Since the evaporation was not intense during the experiment, the amount of powder produced per run can be even larger if the size of reactor would increase. The following powders were synthesized: $CaMnO_3$, $Ca_{0.7}La_{0.3}MnO_3$, $Ca_{0.9}Y_{0.1}MnO_3$, $Ca_{0.8}Y_{0.2}MnO_3$, $Ca_{0.7}Y_{0.3}MnO_3$, $Ca_{0.7}La_{0.3}Ce_{0.2}Mn_{0.8}O_3$, $BaCeO_3$, $BaCe_{0.9}Gd_{0.1}O_3$, $BaCe_{0.85}Gd_{0.15}O_3$, $BaCe_{0.8}Gd_{0.2}O_3$, $BaCe_{0.8}Nd_{0.2}O_3$, $BaCe_{0.8}Sm_{0.2}O_3$. The obtained ashes were afterwards calcined depending on the composition, at temperatures 800–1010 °C, for 2–4 h.

2.2. Characterization

X-ray analysis was used to identify the crystalline phases as well as lattice parameters of solid solutions of obtained powders. The diffracted X-rays were collected over 2θ range 20–130° using a step width of 0.05° and measuring for 2 s per step. Before measurement, the angular correction was done by high quality Si standard. The obtained data were fitted using peak-fitting program [7]. The Lorentizian function gave the best fit to the experimental data. Lattice parameters were refined from the fitted data using a least square procedure. Williamson-Hall plots were used to separate the effect of the size and strain in the nanocrystals [8].

The specific surface area was measured by Brunauer–Emmett–Teller (BET) method using N_2 absorption at 77 K. Classical chemical analysis was performed to check the true composition of all synthesized powders.

SEM (Zeiss) and TEM (Jeol) microscopy were performed to characterize the morphology and size of the obtained powder particles.

Sinterability test was performed for the first group of the powders, manganates, in the temperature range of 1100–1650 °C, for 2 h.

3. Results and discussion

The work carried out recently was mainly concentrated on powder synthesis procedure, with the aim to find the convenient and reliable method which will at the same time be experimentally simple, cost effective and give high yield of synthesized powders. We also put an accent on the amount of powder produced per run.

Glycine nitrate process (GNP) [5] fulfilled our demands and was applied for the synthesis of powders with perovskite type crystal structure. For the reason that reaction between glycine and nitrate components was very intense (burn out process), which caused great portion of the powder to be blown out of the reactor and got lost, the procedure was modified (MGNP).

Glycine nitrate process is based on the self-combustion of the glycine and nitrate mixture, according to the reaction that could be described as

$$2NH_2CH_2COOH + ME^1(NO_3)_3 \cdot 6H_2O + ME^2(NO_3)_3 \cdot 6H_2O + 2O_2 \rightarrow ME^1ME^2O_3 + 22H_2O\uparrow + 4N_2\uparrow + 4CO_2\uparrow$$

which spontaneously occurs at about 180 °C. Glycine plays in this reaction double role, it acts as a fuel and on the other hand as a complexant. By complexing with present cations, their selective precipitation prior to ignition (after the water had been evaporated) is prevented. The reaction is, as mentioned, very intense and needs to be controlled. There are different possibilities to control the reaction rate, and thereby the reaction temperature in order to obtain finer particles and larger specific surface area. We modified the original GNP procedure [5] by replacing partially as discussed above, nitrates by acetates. Acetates are water soluble and are less expensive compared to nitrates of same purity. By applying this method, we managed to produce different powders with more than one dopant cation, of very precise stoichiometry and nanometric particle size. Most of the ashes that are obtained immediately after synthesis were partially amorphous. However, the powders obtained after calcination were all single-phase powders, i.e. solid solutions. Peaks related to isolated dopant oxides or secondary phases were not observed. All of them exhibit perovskite type crystal structure. The example in Fig. 1 is given for Y-doped $CaMnO_3$.

To prove the difference between powders obtained by GNP [5] and MGNP, we synthesized $CaMnO_3$ by both procedures. X-ray patterns of the two ashes (Fig. 2) showed diffraction lines

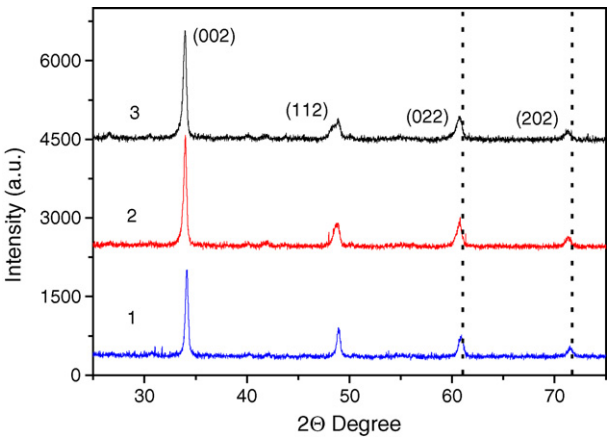

Fig. 1. XRD pattern with different Y-dopant concentration: (1) 10%; (2) 20%; and (3) 30 at.%.

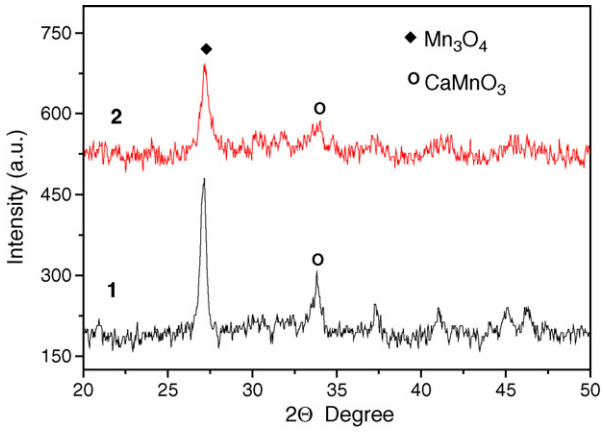

Fig. 2. XRD patterns of $CaMnO_3$ obtained by GNP (1) and MGNP (2) procedure.

at $2\theta = 27,\ 37^\circ$ which belonged to Mn_3O_4 while the one at 2θ = about 33° was the strongest perovskite diffraction line. The only difference in the two XRD patterns was that $CaMnO_3$ ash obtained by GNP was better crystallized, which was to be expected because higher temperatures developed during GNP as compared to MGNP. However, better crystallized powder due to faster growth of crystallites resulted in decreasing of specific surface area.

The ashes, after calcination gave in all cases, as mentioned, single phase powders. In Table 1, specific surface areas and chemical analysis of dopant concentration, in the prepared powders are given. In manganate group of powders (calcined at 800 °C, 2 h), high specific surface area was obtained and seems to exhibit stronger dependence on the dopant type than on the dopants concentration (samples 2 and 6 in Table 1). La-doped powders have lower specific surface area, as compared to Y-doped powders. With increasing Y content, specific surface area of manganates seems to decrease slightly. In accordance with high values of specific surface area, measurement of magnetic properties of these powders indicated that the powders were nanoscale in size, indeed, since the super-paramengetic properties were observed [9]. According to X-ray

Table 1
Specific surface area and dopant concentration

Designed sample composition ($A_{1-x}B_xO_3$)	Surface area (m^2/g)	Dopants content (wt.%)	x in $A_{1-x}B_xO_3$
1. $CaMnO_3$	17.7	–	
2. $Ca_{0.7}La_{0.3}MnO_3$	9.9	19.50 ± 0.40	0.245
3. $Ca_{0.9}Y_{0.1}MnO_3$	17.5	6.13 ± 0.12	0.102
4. $Ca_{0.8}Y_{0.2}MnO_3$	16.3	11.30 ± 0.20	0.195
5. $Ca_{0.7}Y_{0.3}MnO_3$	15.6	16.20 ± 0.30	0.288
6. $Ca_{0.7}La_{0.3}Ce_{0.2}Mn_{0.8}O_3$	13.2	La = 20.80 ± 0.40; Ce = 13.50 ± 0.30	0.289; 0.184
7. $BaCeO_3$	3.6	–	
8. $BaCe_{0.9}Gd_{0.1}O_3$	3.4	4.46 ± 0.06	0.093
9. $BaCe_{0.85}Gd_{0.15}O_3$	3.1	6.51 ± 0.09	0.164
10. $BaCe_{0.8}Gd_{0.2}O_3$	3.5	7.79 ± 0.12	0.180
11. $BaCe_{0.8}Nd_{0.2}O_3$	3.6	7.82 ± 0.12	0.177
12. $BaCe_{0.8}Sm_{0.2}O_3$	3.5	8.86 ± 0.14	0.193

Table 2
Crystallite size and lattice strain in manganates

Composition	Crystallite size (nm)	Lattice strain (E 1000)
$CaMnO_3$	44	1.24
$Ca_{0.9}Y_{0.1}O_3$	44.6	1.5
$Ca_{0.8}Y_{0.2}O_3$	47.8	1.8
$Ca_{0.7}Y_{0.3}O_3$	54	2.2
$Ca_{0.7}La_{0.3}MnO_3$	36	8.5
$Ca_{0.7}La_{0.3}Ce_{0.2}Mn_{0.8}O_3$	32	8.5

measurements, the XRD patterns of all powders looked similar to each other, despite the different amount of dopant. However, a slight difference of peak widths as well as the shifting the peaks toward lower angles with increasing dopant amounts were observed. This indicated the existence of solid solution (Fig. 1) with different crystallite size (Table 2). Microstructure size–strain analysis showed both crystallite size and crystallite strain increase with dopant insertion into perovskite structure. In cerate group of powders (calcined at 1010 °C, 4 h), specific surface area almost does not change, neither with cation type nor with the dopants concentration, although the concentration of dopants was doubled (samples 8 and 10, Table 1). It seems that with increasing calcination temperature, specific surface area decreases drastically, and all other factors influencing specific surface area are masked.

Chemical analysis data (Table 1) show very good agreement between designed and true composition of all synthesized powders.

Since the synthesized compositions are meant to be solid solutions of host compound CeO_2 and the dopant oxide, it is expected that the lattice parameter, a_o, will be related to dopants concentration. Lattice parameters were calculated for all the calcined powders. The results are presented in Figs. 3 and 4 as the dependence of lattice parameters on dopants concentration (x), as well as (Fig. 5), on the dopants cation radii (Ba^{2+} −1.34 Å; Ce^{4+} −0.920 Å; Gd^{3+} −0.938 Å; Sm^{3+} −0.964 Å; Nd^{3+} −0.995 Å; La^{3+} −1.016 Å).

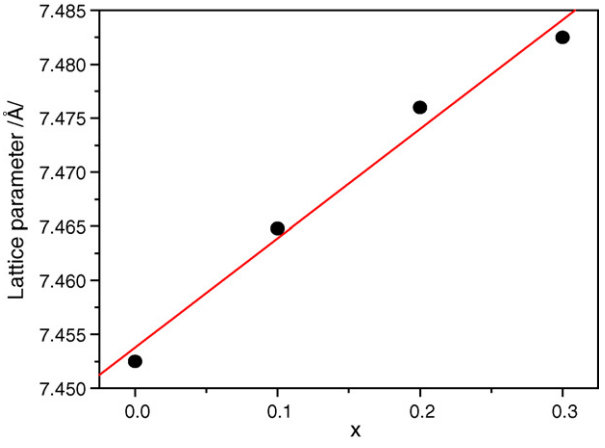

Fig. 3. Lattice parameters of Ca_{1-x} Y_xMnO_3 as a function of Y.

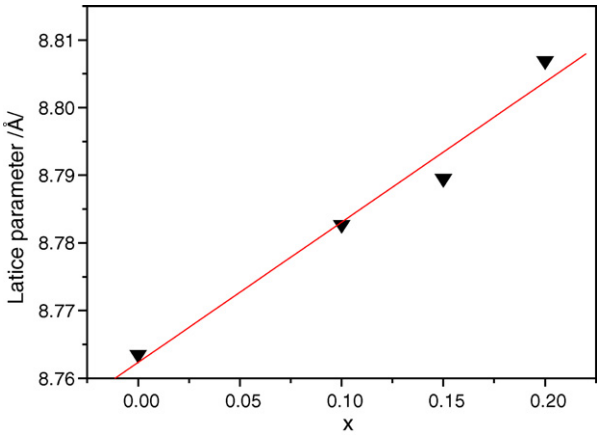

Fig. 4. Lattice parameters of $BaCe_{1-x}Gd_xO_3$ as a function of x.

In $CaMnO_3$ doped with Y^{3+}, lattice parameters obey Vegard's law as shown in Fig. 3. The same was found for lattice parameter dependence on Gd concentration in Ba-cerates. The results on lattice parameters of Ba-cerates on ionic radii of dopants are given in Fig. 4. Data in Figs. 4 and 5 are very important since phase diagrams are not always known, for they prove, too, that single phase powders are obtained.

Since it is very important [10] to produce nanoscale powders which are going to be used for SOFC, because conductivity of nanocrystalline grain boundary regions is higher than in the case of micrometer size grains microstructure [10], SEM and TEM analyses of synthesized, calcined powders were performed. All powders were nanometric in size, which is illustrated in Figs. 6 and 7 for $Ca_{0.9}Y_{0.1}MnO_3$ and $BaCe_{0.8}Gd_{0.2}O_3$ powders, respectively, obtained after calcining. The size of Ca-manganate particles was less than 50 nm in size, which is illustrated in TEM (Fig. 6) for $Ca_{0.9}Y_{0.1}MnO_3$ powders obtained after calcining at 800 °C, 4 h. Insert picture in the right side shows the typical electron diffraction image of the nanocrystal surface which appears disordered, or even amorphous. This matches the XRD results, where short-range order of

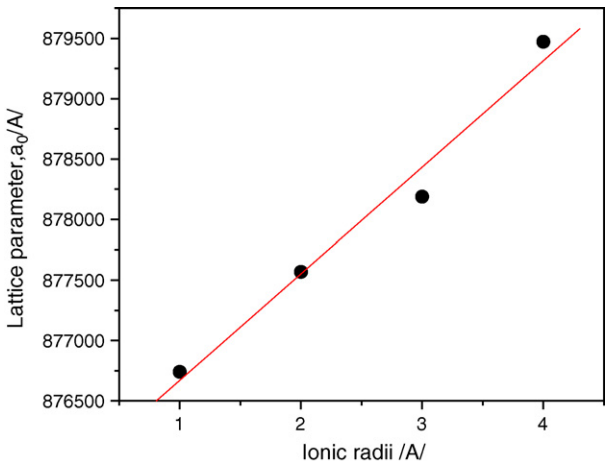

Fig. 5. Lattice parameter of $BaCeO_3$ as a function of ionic radii of dopants (Ce^{4+}, Gd^{3+}, Sm^{3+}, Nd^{3+}).

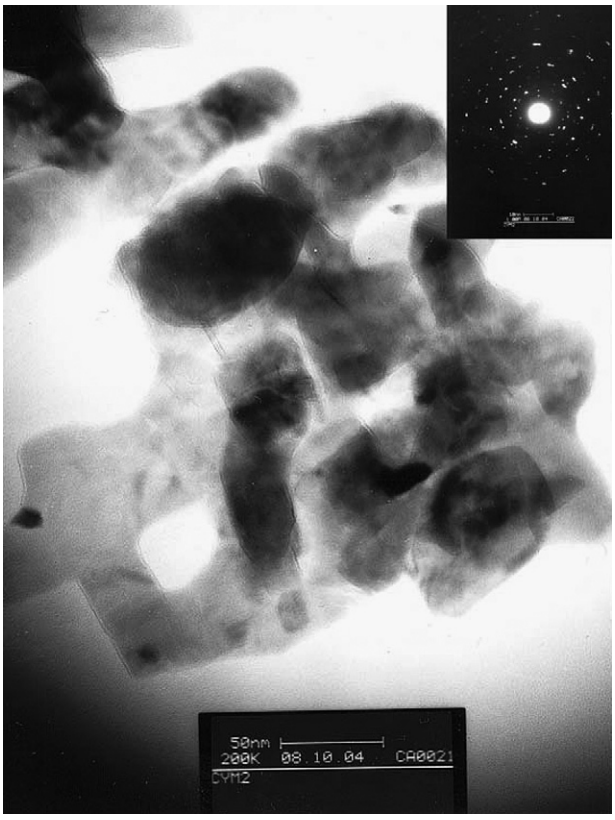

Fig. 6. TEM micrograph with electron diffraction pattern of $Ca_{0.9}Y_{0.1}MnO_3$ calcined at 800 °C, for 2 h.

nanoparticles exhibits diffraction patterns with X-ray peak broadening (Fig. 1).

On the other hand, the size of particles of $BaCe_{0.8}Gd_{0.2}O_3$ after calcinations at 1050 °C, 4 h, lies in the range of 80–100 nm. It is also obvious form Fig. 7, that cerate particles have already been sintered during calcination, which is in accordance with the results obtained for the specific surface area (Table 1), contrary to managante particles that are calcined as mentioned, at much lower temperature.

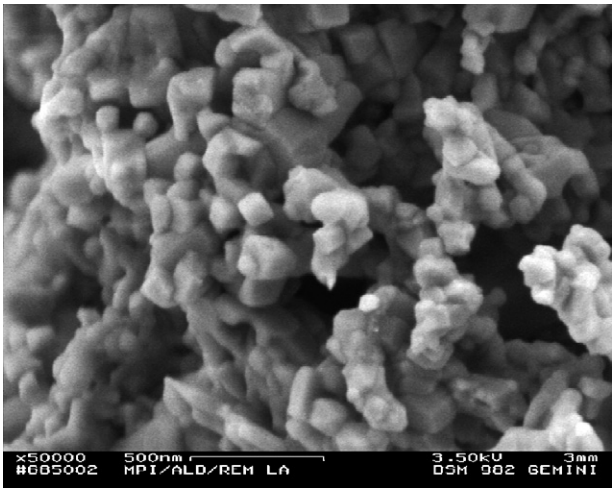

Fig. 7. SEM micrograph of $BaCe_{0.8}Gd_{0.2}O_3$ powder calcined at 1010 °C.

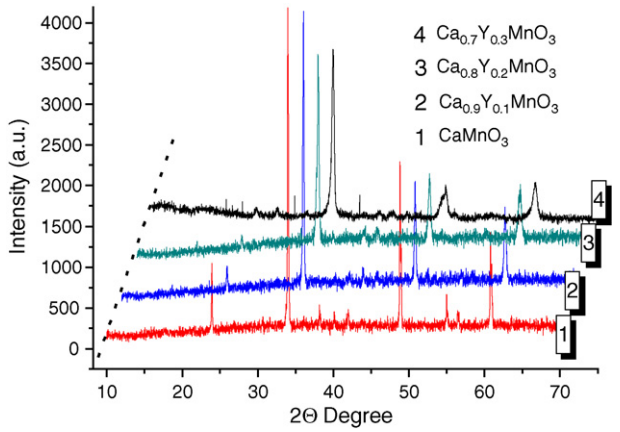

Fig. 8. XRD patterns of $Ca_{1-x}Y_xMnO_3$ sintered at 1150 °C.

Table 3
Sintered densities of mangantes and optimum sintering temperatures

Composition	Density (g/cm^3)	Volume shrinkage (%)	Optimum sintering temperature (°C)
$CaMnO_3$	4.54	50.0	1250
$Ca_{0.9}Y_{0.1}MnO_3$	4.48	55.1	1200
$Ca_{0.8}Y_{0.2}MnO_3$	4.40	–	1150
$Ca_{0.7}Y_{0.3}MnO_3$	4.84	53.6	1150
$Ca_{0.7}La_{0.3}MnO_3$	5.20	–	1350

Sinterability test was performed for the first group of the powders, manganates, in the temperature range of 1100–1650 °C, 2 h. In Table 3, optimum sintering temperatures at which full densities were achieved (over 99% TD) are given. Doping with Y brings about decreasing of sintering temperature, as compared to pure $CaMnO_3$, which is lower than published in [11] and is in accordance with data [12,13] published for active, fine powders. It is also to observe that sintering temperature decreases with increasing Y concentration. Introducing La cations into the Ca manganate lattice obviously results in the increasing sintering temperature which will be studied in detail [14].

X-ray pattern of sintered samples doped with Y showed that the compositions remained single phase after sintering in cases of lower dopant concentration. Samples sintered with 30% of yttrium dopant at 1150 °C (Fig. 8), show the appearing of a new phase (Mn-oxide) indicating that solid solution is unstable at this temperature. This trend is also observed in case of $Ca_{0.7}La_{0.3}MnO_3$ solid solution.

4. Conclusion

Glycine nitrate process (GNP) was modified (MGNP) by partial substitution of nitrates for acetates. The combustion process proceeded very smoothly. Powders with perovskite type structure with cation dopants on A as well as on B sites, or both, were synthesized. Loss of powder during synthesis was negligible. The amount of 100 g of powder was produced per run. Very precise stroichiometry was obtained in accordance with tailored composition. Powders were very active, clean, single phase and nanometric in size. It should be again pointed out that by applying this method

- Large amount of powder can be produced in a very short time
- Single phase nanopowders with high specific surface (among highest published) area are obtained
- No intermediate phases were detected
- Instrumentation is very simple
- Very precise control of stoichiometry is possible all over the batch
- The method is flexible of forming complex compositions

Sintering test for manganates showed that full density was achieved at lower sintering temperatures.

Acknowledgements

The authors are grateful for the support to the Natural Sciences and Engineering Council of Canada, to Alexander von Humboldt Foundation, Germany, Max-Plnck Institute PML, Stuttgart, and the Ministry of Science, Environmental Protection of Serbia.

References

[1] B.C.H. Steele, Materials for IT-SOFC stacks, Solid State Ionics 134 (2000) 3/20.
[2] B.C.H. Steele, Materials science and engineering; the enabling technology for commercialisation of fuel cell systems, J. Mater. Sci. 35 (2001) 1053–1068.
[3] O. Yamamoto, Solid oxide fuel cells: fundamental aspects and prospects, Electrochim. Acta 45 (2000) 2423–2435.
[4] S.M. Haile, Fuel cell materials and components, Acta Mater. 51 (2003) 5981–6000.
[5] L.A. Chick, L.R. Robertson, G.D. Maupin, J.L. Bates, L.E. Thomas, G.J. Exarhos, Glycine-nitrate combustion synthesis of oxide ceramic powders, Mater. Lett. 10 (1999) 6–12.
[6] Y.-J. Yang, T.-L. Wen, H. Tu, D.-Q. Wang, J. Yang, Characteristics of lanthanum strontium chromite prepared by glycine nitrate process, Solid State Ionics 135 (2000) 475–479.
[7] Power Cell program by W. Kraus and G. Nolze, BAM Berlin, Germany.
[8] G.K. Williamson, W.H. Hall, Acta. Metall. 1 (1953) 22.
[9] V. Spasojevic, V. Kusigerski, S. Boskovic, M. Vlajic, V. Krstic, M. Mitric, B. Matovic, Magnetic properties of nanosized mixed valence manganates La0.3Ca0.7$Mn_{1-x}Ce_xO_3$ ($x = 0$; 0.2), Solid State Commun., in press.
[10] M. Oljaca, R. Maric, S. Shanmugham, A. Hunt, Nanomaterials for solid oxide fuel cells, Am. Ceram. Soc. Bull. 82 (2003) 38–40.
[11] C. Moure, M. Villegas, J.F. Fernandez, J. Tartaj, P. Duran, Phase transition and electrical conductivity in the system $TMnO_3$-$CaMnO_3$, J. Mater. Sci. 34 (1999) 2565–2568.
[12] L.M. Rodriguez-Martinez, H. Ehrenberg, J.P. Attfield, Cation size effects in high-tolerance factor $Ln_{0.7}Mo_{0.3}MnO_3$ perovskites, J. Solid State Chem. 148 (1999) 20–25.
[13] D. Ian, Fawcett, E. Joseph, I.V. Sunstrom, M. Greenblatt, Structure, magnetism and properties of Ruddlesden-Popper calcium manganates prepared from citrate gels, Chem. Mater. 10 (1998) 3643–3651.
[14] S. Boskovic, B. Matovic, manuscript in preparation.